ELSEVIER

Contents lists available at ScienceDirect

Planetary and Space Science

journal homepage: www.elsevier.com/locate/pss





A study of an interstellar object explorer (IOE) mission

S. Alan Stern ^{a,*}, Silvia Protopapa ^a, Matthew Freeman ^b, Joel Wm. Parker ^a, Mark Tapley ^b, Darryl Z. Seligman ^c, Caden Andersson ^d

- ^a Southwest Research Institute 1050 Walnut St., Suite 300 Boulder, CO, 80302, USA
- ^b Southwest Research Institute 6220 Culebra Road San Antonio, TX, 78238, USA
- ^c Cornell University 122 Sciences Drive Ithaca, NY, 14853, USA
- ^d Custom Microwave Inc. 4 Boston Court Longmont, CO, 80501, USA

ARTICLE INFO

Keywords: Comets Interstellar objects Interstellar comets Space missions

ABSTRACT

The first discoveries of Interstellar Objects (ISOs), i.e., small bodies moving through our Solar System on high-speed hyperbolic orbits, occurred in 2017 and 2019, decades after ISOs were first predicted. The scientific value of ISOs is high, as they represent samples, most likely planetesimals, from other solar systems. A significant increase in the rate of ISO discoveries is expected in the late 2020s and in the 2030s owing to the advent of several new observing capabilities enabling more routine ISO detections. Here we investigate how a space mission to reconnoiter an ISO can be designed, including discussions of the scientific objectives and payload for such a mission, its unique mission design aspects, and some preliminary spacecraft and payload considerations, all in support of possible proposals to conduct such a mission in the 2030s.

1. Introduction

The discoveries of objects traversing our Solar System with substantial hyperbolic excess velocities, thereby making them on unbound orbits relative to the Solar System (Williams et al., 2017; see also e.g., Meech et al., 2017), proved longstanding predictions that the galaxy should be awash in such objects (e.g., Sekanina, 1976; McGlynn and Chapman, 1989; Stern, 1990; Francis, 2005) which we referred to as ISOs, or InterStellar Objects). ISOs are of high scientific interest because they provide chemical and physical samples from other solar systems. The ESA Comet Interceptor mission (Snodgrass and Jones, 2019) now in build phase plans to explore a long period (Oort Cloud) comet but has also reserved the option of perhaps instead exploring an Interstellar Object if the opportunity presents itself.

We report here on a project to study how a purpose-built robotic ISO flyby reconnaissance mission, called the Interstellar Object Explorer (IOE), which is of modest (i.e., NASA Discovery mission, so <\$1B) cost can be carried out with current spaceflight technology. Our study included the development of the scientific objectives for such a mission, the development of an accompanying Science Traceability Matrix (STM), and a derived payload that spans the STM's key objectives. We then conducted mission trajectory design using the constraints of feasible flight times, existing launch vehicles, and a restriction to solar

powered spacecraft. From that mission design we then derived some key spacecraft requirements. In what follows we describe each of these study elements.

2. ISO population studies

In this section we present an overview of previously developed methodologies to simulate the population of ISOs, in preparation for the mission design work we present later.

2.1. Background

Cook et al. (2016) presented the first detailed simulation of ISOs with the objective of making predictions for the population that would be detected with the forthcoming Rubin Observatory Legacy Survey of Space and Time (LSST; Ivezić et al., 2019). Previously, Moro-Martín et al. (2009) had performed a detailed estimate of the spatial number density based on the non-detections of interstellar objects to date. Specifically, Cook et al. (2016) populated a 1000 AU cube centered on the Sun with synthetic ISOs with random initial velocities and positions and integrated their trajectories to incorporate the effects of gravitational focusing. Cook et al. also demonstrated that macroscopic ISOs should be decoupled from interaction with the ambient interstellar medium

E-mail address: alan.stern@swri.org (S.A. Stern).

^{*} Corresponding author.

kinematically, and therefore should exhibit the same kinematic distributions as their parent stellar populations. To account for the Sun's peculiar velocity with respect to the local standard of rest, Cook et al. subtracted the galactic local standard of rest velocity from the velocity vector of each ISO.

Cook et al. then implemented a realistic set of LSST detectability criteria specifically requiring (1) that the minimum magnitude of the ISO was brighter than a specified sky survey limiting magnitude, (2) that the solar elongation was less than 18° , and (3) that the airmass was less than 2 as observed from the LSST observatory site at Cerro Pachon, Chile. They also incorporated the effects of both asteroidal ISOs and empirically motivated prescriptions for cometary brightening as a function of heliocentric distance. Based on the estimates of the spatial number density from Moro-Martín et al. (2009), Cook et al. (2016) estimated that the LSST would detect \sim 0.001–10 ISOs through a 10-year lifetime with their synthetic populations.

Subsequently, Engelhardt et al. (2017) updated the spatial number density of ISOs based on non-detections with surveys Pan-STARRS1, the Mount Lemmon Survey, and the Catalina Sky Survey. They produced synthetic populations of ISOs and then ran these objects through synthetic surveys to assess the upper limits on their interstellar number density. Engelhardt et al. then generated 1.7 billion random positions of ISOs within a 50 AU sphere centered on the Sun, assigned each random velocities, and integrated their trajectories through the Solar System. For detailed distributions of orbital elements for this synthetic population, see their Fig. 2.

When the first ISO, 1I/2017 U1 ('Oumuamua), was discovered in 2017, the estimates of the spatial number density of asteroidal ISOs were updated to $\sim 0.1-0.2/AU^3$ (Do et al., 2018). Since the discovery of 'Oumuamua, there have been several studies that generated synthetic galactic populations of ISOs to make predictions for the population that will be detected with the LSST given these revised spatial number densities. For example, Seligman and Laughlin (2018; SL18) generated a synthetic population using a similar technique to the Engelhardt et al., (2017) methodology. They then incorporated LSST observability criteria that was more like those developed by Cook et al. (2016). SL18 argued that of the ISO population that would be detected by the LSST, there would be ~10 years between objects with approaches to Earth sufficiently close to enable a space based in situ examination. To generate the synthetic population, their main difference was that instead of generating random positions and velocity vectors, SL18 assumed that the galactic population of ISOs exactly mimicked the kinematics of a given stellar population. They assumed that the ISOs had kinematics like solar-type stars. This generated initial conditions for the Galactic velocity vector of the synthetic objects. They then performed a multi-dimensional Monte Carlo integration over (1) the kinematic velocity distribution of stars, (2) impact parameter, (3) rotation angle, and (4) the location of Earth at the initialization of the simulation. It is important to note that these simulations assumed that every synthetic object had the same absolute magnitude as 'Oumuamua and incorporated no cometary brightening.

Synthetic population models were further developed by Hoover et al. (2022) who performed a more rigorous and higher-resolution simulation of the population of ISOs with more refined estimates of the observability criteria for the LSST. They then presented population statistics for observable quantities of trajectories for both the population that would be detectable with the LSST and the population that would be reachable with various estimates of impulsive ΔV . Their methodology was like SL18, but utilized more stringent LSST observability criteria. Moreover, Hoover et al. (2022) showed how the sky distributions of incoming trajectories would vary as a function of the assumed stellar kinematics.

Marčeta (2023) then developed an entirely analytic method to generate synthetic populations of ISOs. They labeled this method the "probabilistic method" as opposed to the previous Monte Carlo approach labeled the "dynamic method." Their probabilistic method

incorporates the effects of gravitational focusing and can incorporate any background assumed kinematic distribution for the galactic population of ISOs. Because of the analytic properties of the method, the method is several orders of magnitude more computationally efficient than the dynamic method, and can trivially generate population statistics for various assumed stellar kinematics of the population. Then Marčeta and Seligman (2023) implemented this dynamic method with a stringent LSST survey simulation. From this, they predicted the orbital elements and physical properties that the LSST would detect for a range of populations of asteroidal inactive ISOs with varying albedo, size frequency distributions and assumed stellar kinematic distributions.

2.2. Initial conditions

In this paper, we implement the same methodology as Hoover et al. (2022) to simulate the population of ISOs. Because our aim was not to generate population level statistics for multiple assumed kinematics and size-frequency distributions (SFDs), the dynamic method was appropriate for this study. Unlike Hoover et al. (2022), we propagate the trajectories of the initial conditions analytically. We assumed that the ISO kinematic distribution mirrors those of solar-type stars. See Section 4 for more details.

Our detectability criteria for LSST are much more constrained than Hoover et al. (2022) and Marčeta and Seligman (2023). For the purposes of this work, we assume that ISOs are "detectable" if they have heliocentric distances <2 AU (i.e., the nominal solar distance where an interstellar object brighter than 'Oumuamua would be discoverable by the LSST). This is admittedly a crude simplification. However, for the purposes of this paper we aimed to investigate the feasibility of multiple rendezvous pathways to a population of ISOs, despite the detectability criteria. Moreover, we intentionally implemented a generous detection limit as a loose feasibility criterion in order to calculate statistics allowing for larger targets and/or detection via cometary activity. Further still, the size-frequency-distribution of the ISOs is unconstrained (since no spatial number density can be inferred for 2I/Borisov), so this is not physically unmotivated. Future work can refine these estimates, but that is outside the scope of our present work.

2.3. Conversion from simulated detection fractions to detection rates

Because we generate a synthetic population of ISOs, their trajectories represent a steady state distribution of objects passing through a sphere centered on the Sun with an assumed radius R. For a given simulated population, we can convert a percentage of objects that are detectable, to an expected rate of detection.

The first step in that calculation requires the spatial number density of ISOs. We set this parameter to $0.1/\mathrm{AU}^3$ as previously estimated, but the detection rate scales linearly with this number density, so extrapolating our results to other number densities is straightforward.

The second calculation step requires the typical velocity of ISOs passing through a sphere surrounding the Sun. Typical interstellar bodies have velocities relative to the Sun at infinity (V $_{\infty}$) of 20–40 km/s. ISOs then speed up as they fall toward their solar periapse, but they also slow down afterwards leaving the solar potential well.

To model the residency time (i.e., the time crossing the sphere), we took V_∞ and impact parameter for each ISO, derived the Keplerian elements of its Sun-centric hyperbolic orbit, and calculated time between entry into and exit from the radius R sphere. We compiled the distribution of residency times within the sphere; see Fig. 1. The detection rate is then estimated by multiplying the number density by the volume of the sphere, dividing by the residency time, and multiplying by the fraction of ISOs detected. For our study, the detection rate amounted to 15.5 ISOs per year, reasonably consistent with estimates for the detection rate LSST will produce given our simplified detection criteria.

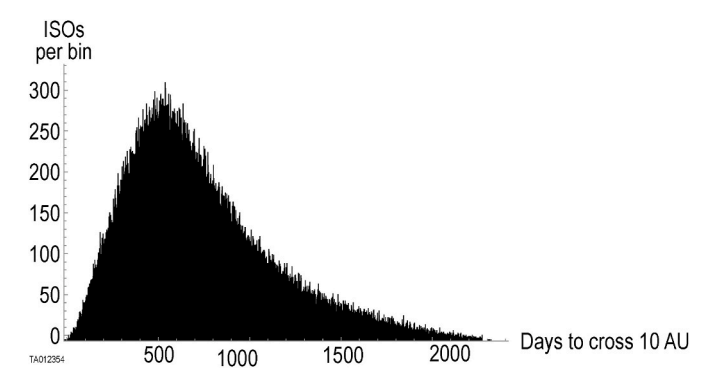


Fig. 1. Distribution of time in days for ISOs in this study to cross 10 AU radius sphere centered on the Sun. Vertical axis is the number of ISOs per 1-day bin. This ISO kinematic distribution matches the kinematic distribution of Sun-like stars, biased by the Sun's velocity relative to the Local Standard of Rest. Keplerian Sun-centric trajectories are assumed, i.e., with no interaction with the planets.

3. Scientific background, goals and objectives

ISOs represent the leftovers from the formation of planetary systems around other stars. As such, their study offers critical new insights into the chemical and physical characteristics of the disks from which they originated. Additionally, a comprehensive analysis of their composition, geology, and activity will shed light on the processes behind the formation and evolution of planetesimals in other solar systems. Close encounters with small bodies in our solar system have vastly enhanced our understanding of these objects, contextualized our ground-based observations, and advanced our knowledge of planetesimal formation models. Similarly, a close flyby of an ISO promises to be equally transformative. It stands as the logical next step in exploring the early history of both our Solar System and exoplanetary systems.

As described above, to date, two ISOs have been identified. The first of these, 'Oumuamua, was discovered in 2017 by the Pan-STARRS1 telescope system (Williams, 2017; Williams et al., 2017). The second, 2I/Borisov, was discovered in 2019 by amateur astronomer G. Borisov (2019). Their interstellar origins were confirmed by their strongly hyperbolic trajectories through the Solar System. Although both objects originate from outside our Solar System, they exhibit remarkable physical differences.

'Oumuamua did not show any direct signs of cometary activity, despite being observed in numerous ways at a distance of just 1.22 AU from the Sun (Meech et al., 2017; Jewitt et al., 2017; Bannister et al., 2017; Knight et al., 2017). In contrast, Borisov displayed clear cometary activity (Jewitt and Luu, 2019; Fitzsimmons et al., 2019; Jewitt et al., 2020). This is believed to have started at a heliocentric distance typical for the onset of water-ice sublimation in comets, approximately 4.5 AU (Jewitt and Luu, 2019). However, Borisov distinguishes itself from the comets that originate in our Solar System because its carbon monoxide to water gas ratio is approximately 173%, which is over three times the ratio measured for any comet within the inner Solar System (Bodewits et al., 2020; Cordiner et al., 2020; Yang et al., 2021). Moreover, its level of sunlight polarization was higher than what is typically measured for Solar System comets (Bagnulo et al., 2021). Unlike the case of Borisov, the lack of cometary activity in 'Oumuamua aided in determining its extreme aspect ratio (6:6:1, Mashchenko, 2019). The disparities between 'Oumuamua and Borisov may indicate differences in the planetary systems from which they originated.

Despite the measurements recounted above, very little is known about the composition, physical makeup, and outgassing activity of these and other ISOs.

3.1. Science goals

The Interstellar Object Explorer (IOE) mission we have studied is designed to explore an ISO at close range for the first time. Its Science Goals (SGs) are:

SG1. Determine the composition of the ISO to provide insights into its origin and evolution. Characterizing the composition and physical properties of materials on and within an ISO is vital to our understanding of the initial conditions in the ISO's host solar system, the nature and evolution of its materials, as well as setting constraints on the processes responsible for planetesimal formation. Compositional studies of primitive objects in our Solar System, such as comets, asteroids, and Kuiper Belt Objects (KBOs)—which serve as the primary comparatives to ISOs—have been instrumental in shedding light on the early history of our Solar System. For instance, the compositional characterization by the NASA New Horizons mission of the KBO, Arrokoth, played a key role identifying gravitational collapse of pebbles in the presence of protosolar nebular gas as its mechanism of planetesimal formation (Stern et al., 2019; McKinnon et al., 2020; Grundy et al., 2020; Stern et al., 2023). Along these lines, the ESA Rosetta mission's compositional analysis of 67P/Churyumov-Gerasimenko's (hereafter 67P) surface revealed the presence of aliphatic organics (Raponi et al., 2020). This discovery holds significant implications for the evolutionary history of the early Solar System and suggests that comets serve as an evolutionary bridge between interstellar material and our Solar System.

SG2. Determine or constrain the nature, composition, and sources of the ISO coma activity and determine the processes responsible for observed activity. Cometary comae typically form as a result of ice sublimation induced by insolation. This sublimation causes gas to flow outward, carrying grains from the nucleus into the coma. These grains predominantly consist of dust and refractory organics, though some may be purely ice grains. The NASA Deep Impact eXtended Investigation (DIXI, A'Hearn et al., 2011) obtained a close-up examination of comet 103P/Hartley 2 at 1.06 AU from the Sun, revealing a highly active nucleus with bright jets rich with nearly pure water-ice grains and dust (A'Hearn et al., 2011). The spatial distribution of carbon dioxide, water-ice, and dust were strongly correlated, leading to the conclusion that CO2 sublimation dominates the comet's activity (A'Hearn et al., 2011; Protopapa et al., 2014). Apart from sublimation, other mechanisms could drive distant comet activity, including latent heat release from the amorphous-to-crystalline water-ice transition (Prialnik et al., 2004). The comprehensive monitoring of comet 67P by the Rosetta mission, has provided detailed insights into the various mechanisms driving cometary activity and the interplay between them. These include sublimation of ice as well as fracturing and cliff erosion, which result from the accumulation of thermal stress due to variations in solar energy on both daily and seasonal scales. Therefore, activity is strongly dependent on both solar energy and the comet's own physical characteristics (Marschall et al., 2020; El-Maarry et al., 2019; Vincent et al., 2019). By characterizing the composition and spatial distribution of an ISO's coma, IOE can directly determine the primary components of its target ISO, identify the mechanisms behind coma activity, and deepen our insights into the composition and processes extant in its protoplanetary formation disk, where planetesimals like it were forming. For instance, investigation of the composition of cometary comae (CO/CO₂/H₂O gas content and broad band visible colors) led to the understanding that cometesimals that might later have assembled into comets, formed between the CO₂ and CO snow lines (A'Hearn et al., 2012; Jewitt, 2015). Furthermore, comparing the physical properties (i. e., the chemical composition, size distribution, type of mixing) of ices and refractories in the coma with those on the surface can provide insights into potential processes that may have modified the surfaces.

3.2. Derived science objectives

The two SGs just described in turn motivate four Science Objectives

(SOs) for an IOE mission. These are:

SO1: Search for and characterize windows into the ISO's subsurface geology. This is accomplished by determining the distribution of observable (a) subsurface albedo structures and (b) exposed surface and subsurface features such as craters and scarps, and sites of past or present activity. SO1 requires a panchromatic visible-wavelength imager with arcsecond-class angular resolution and high dynamic range.

SO2: Determine the colors, compositions, and photometric properties of the ISO's surface and subsurface. This will be achieved by assessing the (a) distribution of color units at different spatial scales, (b) distribution of compositional units, including minerals, ices, salts, organics, and other materials at different spatial scales (e.g., $\rm H_2O$ ice, $\rm CO_2$ ice, $\rm NH_x$ salts, aliphatic organics), and (c) disk resolved photometric properties of selected regions of interest. A visible-wavelength imager with a minimum of three filters is needed, along with an infrared imaging spectrometer that spans the 1–2.5 μm wavelength range, possibly extending up to 4 μm , with a resolving power of at least 100 to identify and characterize broad compositional absorption bands.

SO3: Characterize the ISO's chemical and physical properties of the ice, dust, and gases in its coma. This can be achieved by constraining a) the production rates for parent molecular gas species in the coma (e.g., H₂O, CO, CO₂, N₂, O₂, CH₄) b) the abundance, path length, purity, mixing ratio of ices and refractories in the coma, and c) the microphysical properties of the dust (ices and refractories) in the coma. In addition to the previously mentioned instruments, an ultraviolet (UV) spectrometer spanning the wavelength range of 700-1970 Å with a spectral resolution of ≤20 Å is essential in satisfying SO3. Similar UV spectrometers have been used to detect or set upper limits for such species without requiring appulse absorption from a background star (Feldman et al., 2007, 2015, 2016). SO3a requires modeling spectroscopic emission line intensities in the UV and IR spectral range. SO3b entails modeling the continuum and any absorption bands attributable to ices and refractories across a broad wavelength spectrum via radiative transfer models (e.g., Protopapa et al., 2018). Analysis of the coma phase function at least at one wavelength covering a large phase angle range (phase angle range 0-120 deg) provides a tool to investigate the nature of cometary dust (SO3c, Bertini et al., 2017). Some of these SO3 measurements can be obtained from Earth- and space-based observatories, though at lower spatial resolution; for example, JWST can be used to make excellent measurements of H2O, CO and CO2 if the ISO's apparition is within JWST visibility and tracking constraints. There is already a standing target of opportunity JWST Cycle 2 program to measure production rates of H₂O, CO and CO₂ for the next ISO (Meech et al., 2023). However, spectral detection of some species such as O2 require UV observations not obtainable with JWST and Earth-based observatories, and also require short length scale resolution in the inner coma that require the spatial resolution provided by a close encounter mission like ISO.

SO4: Understand the nature of the ISO coma activity. This objective can be met by a) assessing the types and distribution of coma structures (e.g., sources of vents, plumes, jets, cliff collapse, mass wasting processes) and, b) constraining the chemical nature of the coma structures (e.g., $\rm H_2O$, $\rm CO_2$, $\rm CO$). To achieve this objective, both a panchromatic visible-wavelength imager and UV and infrared imaging spectrometers are essential.

4. Mission design

Design of any practical mission to intercept an ISO is driven by several important constraints which do not apply to most interplanetary mission trajectory designs. Chief among these is the ephemeral nature of ISO targets, which approach the Solar System generally undetected until they are close to the inner edge of the asteroid belt, as well as their substantial hyperbolic velocity, which means they pass through the Solar System and become unreachable quite soon after detection.

As noted above, for this study we set the detectability limit at 2 AU. We simulated all ISOs with a closest solar approach of 10 AU or less.

Although most of those will remain undetected due to our 2 AU or closer detectability criterion, the larger 10 AU closest solar approach upper limit ensures that we compensate correctly for the effects of gravitational focusing by the Sun. We used a velocity distribution at infinite distance consistent with the velocity distribution of class G (Sun-like) stars biased by the Sun's velocity with respect to the local standard of rest. The Sun's gravitational focusing has more impact on the trajectories of the slower-moving objects, and hence the detected population (those passing within 2 AU of the Sun) have a lower mean velocity than the overall population. Both velocity distributions are shown in Fig. 2.

For our modeled population, the detectable subset has a mean approach velocity of $32.14~\rm km/s$, hence the average time within the modeled sphere (of solar radius $10~\rm AU$) is only $770.5~\rm days$. Typically, the most viable intercept trajectory results in a flyby near the middle of this arc, meaning the time between detection of the ISO and intercept is often compressed to considerably less than one year. Although the approach directions are concentrated in one area of the sky due to the Sun's velocity vector, the random distribution in impact parameter direction means that the inclinations of the hyperbolic orbits are distributed from 0° to 180° (this parameter is not affected by the Sun's gravitational focusing nor the detectability limit, which is modeled as a uniform sphere).

The available time between detection and intercept, which is a strong function of many variables specific to the individual ISO, including the positions of the Earth and ISO at the time of its detection, and the ISO's orbit parameters, are powerful constraints on mission feasibility. But at least two other constraints are also appropriate to mention. Heliocentric radius of intercept is the first of these; at very large heliocentric distances (>3 AU) many issues of mission design including spacecraft power subsystem and communications challenges become intractable, thus, we restrict the mission design to require a heliocentric distance at intercept of <3 AU for our study. Second, the relative velocity between spacecraft and the ISO at intercept can have very large values (above 100 km/s) which can make intercept terminal navigation and science data collection quite challenging. For this study, we restricted intercept relative velocity to 100 km/s, which is only $\sim 30\%$ higher than the fastest comet intercept velocity to date.

In order to effectively analyze the frequency of feasible intercepts, we elected to generate an algorithm which optimized the intercept trajectory given the mission constraints discussed above. We then down-selected to the small subset of ISOs for which a feasible intercept trajectory could be created, and evaluated the statistics of this subset.

An early choice we made was to dismiss the possibility of electric propulsion. Although large available IOE ΔV turns out to be a key driver of mission feasibility, we found that given the short warning time constraint from discovery to feasible intercepts, electric propulsion

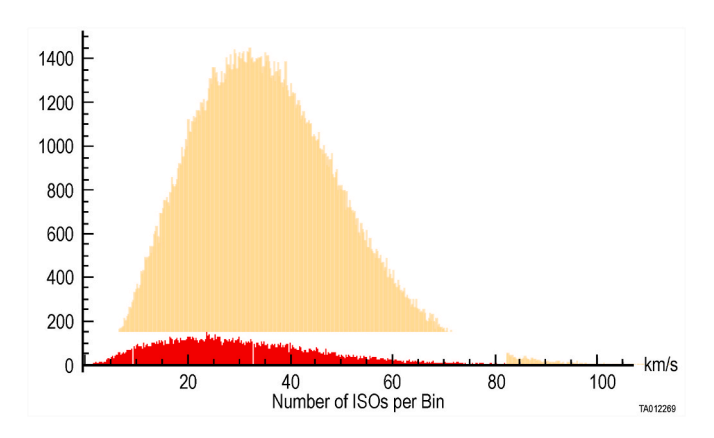


Fig. 2. Velocity Distributions. Velocity distribution of our overall population in yellow, and superposed on this, the velocity distribution of the detectable subset of that population in orange. Vertical axis is number of ISOs per bin, horizontal axis is velocity in km/s.

systems were ineffective because they are all low thrust and they simply require too many months to generate the large ΔV of which they are capable. That limited us to two intercept mission design options: storage on the Earth, with a high-energy (planetary trajectory) type launch soon after detection of the ISO, or launch to a storage on-orbit from which the intercept is commanded following discovery of a suitable target ISO.

Although we were able to generate the greatest number of intercepts of the test population by using an Earth-based launch, we could do so only by assuming an unrealistically short period of 30 days between detection of the ISO and launch. Longer launch delays resulted in a rapidly declining fraction of ISOs which could be reached. We believe that holding a planetary class launch vehicle ready for multiple years until a suitable target is found, followed by a 30-day time constraint from storage to launch, would not be viewed as practical in a NASA mission proposal. We therefore concentrated on mission designs which place the IOE spacecraft into a storage orbit after launch, where it would await a command to affect the ISO intercept.

For the storage orbit, we selected a location at the Earth-Moon L1 point, between the Earth and Moon. This location combines several desirable features: the spacecraft already has almost C3 = 0 in its storage location, so most of its available ΔV can go toward the intercept trajectory; departing L1 is far less expensive in ΔV than departing from geosynchronous orbit; the fall time from L1 to a near-Earth flyby is less than 4 days; the orbit period of the Moon (and hence L1) is short compared to that of the Earth around the Sun, enabling any launch azimuth within $\leq\!28$ days after detection; and finally, maintenance of the IOE spacecraft in its L1 storage orbit is relatively easy, with only infrequent contacts or maneuvers needed for station-keeping. We chose a near-Earth gravity assist altitude of 400 km as the first phase of the intercept, which allows the spacecraft to capitalize on the powered swing-by to strongly leverage the effect of its propellant on its departure V_{∞} from Earth toward the ISO (i.e., we use the "Oberth effect").

Maximum V_{∞} leaving Earth was the driving parameter enabling intercepts. For Earth launch, we had assumed a typical inner-Solar System value of 8.6 km/s, based on a C3 =0 (exactly escape velocity) launch vehicle supplemented by a 3.0 km/s ΔV from the IOE spacecraft itself. The Lunar L1 storage orbit assumed that the same C3 =0 launch vehicle delivered the spacecraft to the L1 storage location, and the spacecraft then uses its 3.0 km/s ΔV capability to depart L1 on a low Earth swingby trajectory, and then add velocity at perigee during the swing-by. Because the spacecraft also has to incorporate any needed inclination change at L1 departure, the final V_{∞} varied from a maximum of 7.35 km/s in the ecliptic down to a minimum 6.72 km/s for a polar Earth departure inclination.

We ran all of our calculations over a period of 10 years to ensure that there were no seasonal, or start-up or shut-down effects on our model ISO population. This also corresponds to the longest loiter duration we chose as reasonable. In either the case of Earth storage or L1 storage, there is ample precedent to show that space systems can, with adequate precautions, be maintained in operable and ready-to-initiate-mission-operations conditions over a decade with a very high probability of mission success.

Given these various mission design constraints, we were able to generate a list of key mission parameters which are technically feasible (i.e., similar numbers having been demonstrated on previous missions) and which we then took as baseline mission parameters. These parameters are shown in Table 1.

Table 1Key mission parameters.

Parameter	Value	Precedent Mission
ΔV Capability	3.0 km/s	Cassini (2.1 km/s)
Minimum Planetary Flyby Altitude	400 km	Galileo (303 km)
Maximum Heliocentric Radius	<3 AU	Juno (5.2 AU)
Flyby Relative Velocity	100 km/s	"Halley Armada" (70 km/s)

For any given ISO in our model population, our intercept trajectory generation algorithm followed a standard sequence. First, it assumed the optimum intercept location would be in the plane of the ecliptic, as these locations were most likely to be reachable given the practical limitation on V_{∞} leaving Earth. Next, we calculated a transfer orbit from Earth's orbit to this location (tangent to Earth's orbit from a departure location on the far side of the Sun from the intercept), which served as the initial estimate of the optimum intercept trajectory. Next, we minimized Earth departure V_{∞} by adjusting date of departure and date of intercept at the ISO, using a steepest-gradient search algorithm.

Finally, we repeated the departure velocity minimization with constraints applied to represent earliest detection date of the ISO and any other mission-related requirements. In particular, we imposed a minimum 3-day period between ISO detection and the maneuver departing lunar L1 storage orbit. (We note that in many cases, the delay will be longer, up to a lunar month, before the Moon is in the correct position to initiate the Earth swing-by, and in all cases, total ISO tracking time prior to the Earth swing-by will be at least the 3 days we imposed plus the almost 4-day "fall time" from L1 to the swing-by. This is seen as adequate to set up an approximate intercept trajectory with small TCMs later able to fine-tune the intercept in response to additional tracking data on the ISO.) An example intercept trajectory with the mission constraints applied appears in Fig. 3.

The above algorithm is intuitive and reliably produces best available intercept trajectories, but analysis of the full population using this sequence of calculations requires substantial computational time. To increase throughput, we re-sequenced the calculations to cull out needless work by successively removing unreachable ISOs from the population under consideration.

Starting with the full population, we thus first eliminated any ISOs which did not penetrate the "detectability sphere." Next, we ran the initial estimate of the intercept at ecliptic crossing and the first optimization to minimize departure $V_{\infty}.$ Any comet which required a V_{∞} above our system capability even without other constraints applied could also be eliminated, since additional constraints would never reduce the requirement. With these reductions applied, the final

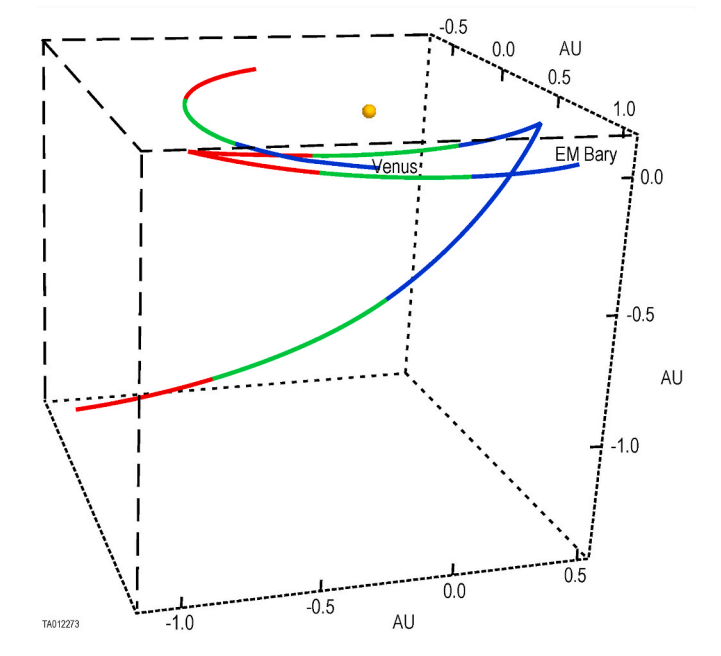


Fig. 3. Intercept trajectory with constraints applied. Departure from Earth-Moon L1 is constrained by detection date, and subsequently by Earth/Moon geometry being correct for departure asymptote after low Earth swing-by. Departure V_{∞} from Earth is 4.529 km/s, which is easily achievable for our spacecraft. Each color band represents 30 days.

optimization applying launch geometry constraints proceeded. As a last step, intercepts not meeting the constraints on maximum relative flyby velocity or on heliocentric radius at intercept were also eliminated. With these process improvements, we are able to analyze a model population of over 200,000 ISOs within a few hours.

Once we had analyzed our model population to determine what fraction of it represented reachable ISOs, we calculated the mean time between reachable ISOs according to equation (1):

$$T_{avg} = T_{model} / (D_{int} \ V_{model} \ P_{feas}) \tag{1}$$

Here, T_{avg} is time between interceptable ISOs, V_{model} is the volume of the sphere containing all of the impact parameters, D_{int} is the expected density of ISOs in interstellar space (0.1/AU³), T_{model} is the time each ISO is within V_{model} (770 days), and P_{feas} is the fractional chance that a given ISO from the original model population is interceptable.

We then converted mean time between intercepts to percent chance of having a viable intercept within a 10-year allowable mission loiter duration using Poisson statistics. By varying the input parameters, we were also able to generate percent chance of an intercept for similar missions using a smaller or larger detection sphere radius and a spacecraft with more or less ΔV capability. The results appear in Table 2 below; our baseline mission is highlighted in green (for reference, the mean time between interceptable ISOs is 3.48 years for the 94.5% odds of success quoted).

We note that in the event that no suitable ISO is found, the ISO mission should have a suitable non-ISO, backup target to explore.

5. Payload

Just as almost every comet and asteroid mission is a first-time visit to a given target, IOE will be a "first and only" visit due to the hyperbolic trajectory of its target. As such, the IOE payload needs to be broad enough to enable discovery of unexpected features and properties, while still being tailored to capture the ISO's properties, likely shared with the various small body types in our Solar System.

The IOE encounter speed is expected to be high, as described in Section 4. The mission science payload needs to be able to meet its observation requirements for these high encounter speeds, as well as for the relatively small diameter of target (perhaps as small as \sim 1 km) and the expected close approach distance of \sim 400 km.

The science objectives discussed above in Section 3 drive us to consider a payload suite with broad, general capabilities for imaging and spectroscopy. The strawman payload is comprised of a panchromatic visible imager, a color imager and IR spectrometer, and a UV spectrometer. Next, we outline the necessary capabilities of each instrument, relevant specifications based on heritage mission instruments of the same types, and how each addresses IOE's science objectives.

5.1. Panchromatic visible imager

This instrument is needed to characterize the geology and photometric properties of the ISO's surface, for measuring light curve and rotational properties, for determining the ISO's shape, mapping structures in its coma, and searching for orbiting satellites or escaping fragments.

We base the concept of this IOE instrument on the L'LORRI imager

Table 2
Trajectory results summary.

Odds of Success (%)		ΔV (km/s)			
		1.7	2.1	3	3.9
Detection Radius (AU)	1.8	45.51%	58.86%	82.45%	93.46%
	2.1	65.05%	78.38%	94.50%	98.85%
	2.5	80.78%	89.99%	98.37%	99.85%
	3	93.75%	97.80%	99.915%	99.998%

on the Lucy mission (Weaver et al., 2023), which itself is based on the LORRI instrument flown on the New Horizons mission (Cheng et al., 2008; Weaver et al., 2008). This imager is a Ritchey-Chrétien optical design, with a 20.8 cm primary mirror feeding a 1024x1024 pixel imaging CCD. The key attributes of this instrument are summarized in Table 3.

5.2. Color imager and IR mapping spectrometer

This instrument is needed for IOE's color imaging and surface composition objectives, such as determining the colors, compositions, and photometric properties of the ISO's surface and its coma particles.

We base this IOE instrument on the L'Ralph instrument on the Lucy mission (Reuter et al., 2023), which itself was based on the Ralph instrument on the New Horizons mission (Reuter et al., 2008; Weaver et al., 2008). The instrument consists of a single telescope that passes light through a dichroic beam splitter to transmit light to two cameras: the Multi-spectral Visible Imaging Camera (MVIC) and the Linear Etalon Imaging Spectral Array (LEISA).

The MVIC color imager has multiple 5024x64 pixel Time Delay and Integrate (TDI) arrays that meet the science requirements for broadband color and composition imaging. The Lucy MVIC has five such color TDI CCDs (violet, green, orange, phyllosilicate, and near-IR) and one panchromatic channel, which has a wider field of view to complement and serve as a backup to the visible imager.

The LEISA hyperspectral imager has a 2048x2048 pixel HgCdTe array operated in push broom mode. It creates a 2-D spatial x 1-D spectral data cube. The key attributes of this instrument are summarized in Table 4.

5.3. UV spectrometer

The ultraviolet spectrometer instrument for IOE measures the UV photometric properties of the surface, measures or sets upper limits on the chemical and physical properties of dust and gas in the ISO coma, and characterizes the nature of the ISO's activity.

This IOE instrument is based on the UV spectrograph (UVS) on the ESA JUICE mission (Davis et al., 2021), which itself is based on the long line of "Alice" UV spectrographs that flew on the ESA Rosetta (Stern et al., 2007), NASA New Horizons (Stern et al., 2008), NASA Lunar Reconnaissance Orbiter (Gladstone et al., 2010), and NASA Juno missions (Gladstone et al., 2017).

The JUICE UVS high-resolution Jupiter-system observing port would not be needed for IOE. The JUICE UVS's 10 kg of shielding for the Jupiter's radiation environment can also be eliminated for IOE.

The instrument's optical design is an off-axis primary in a Rowland circle mount. The detector is a 2-dimensional (2048 spectral x 512 spatial) microchannel plate, with a Caesium Iodide (CsI) photocathode, and cross-delay-line readout. The key attributes of this instrument are summarized in Table 5.

5.4. Payload applicability and other considerations

With this set of instruments, the IOE strawman payload is able to meet the Science Objectives listed in Section 3 as shown in Table 6.

Table 3 IOE panchromatic visible imager attributes.

Attribute	Value
Aperture	20.8 cm
Focal Length	262 cm
FOV	0.29 deg (5.1 mrad)
Pixel Size	1.04 arcsec (5.03 µrad)
Spectral Range	420-795 nm at 50% of peak QE
	380-860 nm at 10% of peak QE

Table 4 IOE color imager and IR mapping spectrometer imager attributes.

Attribute	Value
Overall	
Aperture	75 mm
Focal Length	450 mm
MVIC Imager	
FOV (TDI array)	$8.25 \text{ deg} \times 0.105 \text{ deg}$
Pixel Size	29 μrad
Spectral Range	0.38-0.92 μm
Spectral Resolution	47–550 nm
LEISA Mapping Spectrometer	
FOV	$2.35 \deg \times 3.37 \deg$
Pixel Size	40 μrad
Spectral Range	0.95–3.95 μm
Spectral Resolution	10 nm

Table 5 IOE ultraviolet spectrometer attributes.

Attribute	Value
FOV	$0.1 imes 7.3~ ext{deg}$
Pixel Size (spatial)	0.0092 deg
Pixel Size (spectral)	0.106 nm
Spectral Resolution	0.5-0.8 nm (point source)
	<1.2 nm (extended source)
Spectral Range	50-204 nm

 Table 6

 Science objective/instrument Traceability Matrix.

	Panchromatic Visible Imager	Color Imager	IR Mapping Spectrometer	UV Spectrometer
SO1	X			
SO2	X	X	X	
SO3	X	X	X	X
SO4	X	X	X	X

Two other instruments considered for the IOE payload, but ultimately not chosen were.

- Mass spectrometer. A mass spectrometer would be able to constrain the coma isotopic ratios. That would be valuable information about the parent stellar system where the ISO formed, providing additional data points about the range of chemistry for planetary system formation models. One such mass spectrometer with strong heritage is Rosetta's ROSINA instrument (Balsiger et al., 2007). However, these types of instruments with sufficient resolution have high mass and power specifications, as well as strong spacecraft accommodation and operational requirements, and we determined that one could not be accommodated on the IOE due to associated cost.
- Radio science instrument. A spacecraft's high gain antenna is often used to determine the mass of the target. Then, using the volume as estimated from the camera data (with assumptions about the shape of any unobserved or unilluminated region), the target's bulk density could be computed and perhaps information could be obtained about its gravity field and internal structure. The perturbed motion of the spacecraft near the target leads to perturbed Doppler frequency shifts of the spacecraft's transmitted radio signals recorded on Earth. Perturbing forces acting on the spacecraft are the asymmetric gravity field of the nucleus, third body perturbations, the solar radiation pressure, and the cometary outgassing pressure. The precision of a flyby mass measurement will mainly depend on the Doppler frequency noise level, on the distance between the spacecraft and the target, the flyby speed, the uncertainty of the outgassing pressure of any coma, and of course the size of the target. With likely high encounter speeds, possibly a small (~1 km) target, and uncertain

coma activity, we found that such measurements for an ISO flyby mission are not possible by many orders of magnitude.

6. Spacecraft requirements

Although spacecraft design for the IOE mission has not yet been undertaken, the following requirements to that design can be established.

6.1. Payload requirements

The purpose of the spacecraft bus is to support the IOE mission's scientific payload, delivering it where it needs to go, ensuring sufficient power and data storage are available to conduct observations, and returning data from the observations required to satisfy the mission's scientific objectives. As such, the spacecraft design begins with the requirements shown below. The estimates for the instruments below are based on their most recent heritage designs: Lucy's L'LORRI panchromatic camera and L'RALPH color camera/infrared composition mapping spectrometer, and the Europa Clipper UV atmospheric spectrometer (UVS)

The payload mass, volume, and power estimates for this payload are shown below in Table 7, and include 25% contingency. One significant change for the UVS mass from its Europa Clipper predecessor is the removal of the Tantalum radiation shield plates required for operation in the Jovian environment. This reduces the overall mass of the instrument by approximately 10 kg. The low overall power demand of the instruments and the relative proximity of the spacecraft to the Sun throughout the IOE allow the mission to utilize solar power.

Payload data volume estimates are shown below in Table 8. These numbers assume the flyby lasts at least 20 days around approach and departure, and that the instrument suite will operate continuously during that time, but it is not necessary that each instrument operate continuously at their maximum data rate. Each instrument will have its own onboard data storage, so data can be copied to the spacecraft storage after the encounter without high data rates overwhelming the bus in real time. The data would be returned to Earth at a much slower rate within 12 months after the encounter.

6.2. Spacecraft bus requirements

Aside from supporting the payload, two specific requirements will also heavily drive the design of the IOE spacecraft: pointing capability and $\Delta V.$

As described in the previous section of this paper, the flyby speed of the ISO could be up to $100~\rm km/s$. For a closest approach of $400~\rm km$, the pointing capability for the spacecraft would need to be $14~\rm deg/s$ Based on the known pixel size of each instrument, spacecraft pointing stability (driven by LORRI's half pixel stability requirements) would need to be on the order of $2.5~\rm \mu rad$. These requirements suggest that a dedicated instrument pointing and scan platform will be a superior approach than turning and stabilizing the entire spacecraft. The assumption of a flyby at up to $100~\rm km/s$ with a closest approach distance of $400~\rm km$ and a cometary activity implies the need for a heavy dust shield, which could become a driver for spacecraft and instrument scan platform design.

Table 7Payload mass and volume and power estimates.

Payload Item	Dimensions (cm)	Mass (kg)	Power (W)
LORRI	100 x 25 x 25	15	13.8
Ralph	50 x 50 x 25	40	30.6
Ralph Electronics	30 x 30 x 20		
UVS	35 x 41 x 16	10	14.5
Total		65	58.9

Note: Payload masses and powers include 25% contingency.

Table 8 Payload data volume estimates.

Payload Item	Maximum Data Rate (Mbps)	Encounter Data Volume (GBytes)
LORRI	12.6	20
Ralph	157.1	40
UVS	40	7
Total	N/A	67

Note: Payload data volume estimates include 25% contingency.

As discussed above in Section 4, the large (2–3 km/s) mission ΔV and the impulsive nature of the initial intercept burn to target a flyby, precludes the spacecraft utilizing ion electric propulsion and instead requires a chemical propulsion system. IOE can therefore be accomplished with liquid monopropellant or biprop, or solid rocket motor intercept propulsion; because trajectory corrections additionally require propulsive maneuvers, the spacecraft is assumed to be most mass and cost efficient using a liquid propulsion solution for all ΔV s.

The specific impact hazard environment surrounding the comet is difficult to estimate. The two previously detected ISOs showed very different environments, with Borisov looking fairly typical for a comet but 'Oumuamua having no detectible coma. We assumed a worst-case estimate and extrapolated a Halley-equivalent dust/gas environment to 400 km. We also assumed that the instrument's thermal environments (survival and operational) would not change compared to their heritage instruments and the payload would need to maintain a survival temperature between $-30\ C$ and $+45\ C$ and an operational temperature between $-15\ C$ and $+40\ C$. The IOE mission radiation environment was modeled as a 10-year dwell at the Earth-Moon L1 and resulted in a total ionizing dose of 40 krad (si) and a displacement damage dose of 6 \times $10^{11}\ MeV/g$. The operational life of the spacecraft is set to be 13 years, composed of 10 years of potential loiter, a worst case of 2 years of flight to closest approach, and a worst case of 1 year to downlink data.

6.3. Spacecraft operations

The mission can be divided into three distinct phases: loiter, approach and flyby, and post-flyby downlink.

During the loiter phase, the spacecraft is primarily dormant. Aside from routine spacecraft and payload maintenance, the instruments will only occasionally be powered on to check health and calibrate performance.

Once an interceptable ISO is detected and the spacecraft is put on an intercept trajectory to it, the approach and flyby phase of the IOE mission begins. The primary activities enroute will be spacecraft navigation and course corrections, and flyby rehearsal(s). Flyby observations will be executed with a high level of autonomy to maximize data collection without relying on real-time commanding. We anticipate a worst-case comet encounter distance of 3.3 AU from Earth.

The third phase of the mission is post-flyby data downlink. The goal of this phase is the transmission of the collected flyby data to Earth. We anticipate the use of spacecraft data compression to facilitate the downlink, and assume one 34m DSN antenna can be used to execute the transmission.

7. Summary and conclusions

In this paper, we have summarized study results specifying the scientific goals and objectives, mission design, overarching requirements, and payload complement of a possible mission to an interstellar object (ISO). More detailed work will be needed next to better prepare the mission concept to be proposed to a future NASA mission opportunity, but this report provides the mission's basic objectives, key requirements, and attributes as a starting point.

CRediT authorship contribution statement

S. Alan Stern: Conceptualization, Writing – original draft, Writing – review & editing, Funding acquisition, Investigation, Resources, Validation. Silvia Protopapa: Writing – original draft, Writing – review & editing, Formal analysis, Investigation. Matthew Freeman: Formal analysis, Writing – original draft, Writing – review & editing, Investigation. Joel Wm. Parker: Formal analysis, Writing – original draft, Writing – review & editing, Investigation. Mark Tapley: Formal analysis, Writing – original draft, Writing – review & editing, Investigation, Visualization. Darryl Z. Seligman: Formal analysis, Writing – original draft, Writing – review & editing, Investigation. Caden Andersson: Formal analysis, Writing – original draft, Writing – review & editing, Investigation.

Declaration of competing interest

The authors declare that they have no known competing financial interests or personal relationships that could have appeared to influence the work reported in this paper.

Data availability

The data that has been used is confidential.

Acknowledgements

This work was primarily funded under an internal research grant from the Southwest Research Institute (SwRI). D.Z.S. is supported by an NSF Astronomy and Astrophysics Postdoctoral Fellowship under award AST-2202135. This research award is partially funded by a generous gift of Charles Simonyi to the NSF Division of Astronomical Sciences. The award is made in recognition of significant contributions to Rubin Observatory's Legacy Survey of Space and Time. We thank SwRI's Matt Beasley and Sierra Ferguson for their helpful input on the strawman payload. We thank our two anonymous referees for their very constructive comments on the originally submitted manuscript.

References

A'Hearn, M.F., et al., 2012. Cometary volatiles and the origin of comets. Astrophys. J. 758, 29. https://doi.org/10.1088/0004-637X/758/1/29.

A'Hearn, M.F., et al., 2011. EPOXI at comet Hartley 2. Science 332, 1396. https://doi. org/10.1126/science.1204054

Bagnulo, S., et al., 2021. Unusual polarimetric properties for interstellar comet 2I/ Borisov. Nat. Commun. 12, 1797. https://doi.org/10.1038/s41467-021-22000-x.

Balsiger, H., et al., 2007. Rosina-rosetta orbiter spectrometer for ion and Neutral analysis. Space Sci. Rev. 128, 745–801. https://doi.org/10.1007/s11214-006-8335-3

Bannister, M.T., et al., 2017. Col-OSSOS: colors of the interstellar planetesimal 1I/ 'Oumuamua. Astrophys. J. Lett. 851, L38. https://doi.org/10.3847/2041-8213/ aaa07c.

Bertini, I., et al., 2017. The scattering phase function of comet 67P/Churyumov-Gerasimenko coma as seen from the Rosetta/OSIRIS instrument. Mon. Not. Roy. Astron. Soc. 469. S404–S415. https://doi.org/10.1093/mnras/stx1850.

Bodewits, D., et al., 2020. The carbon monoxide-rich interstellar comet 2I/Borisov. Nat. Astron. 4, 867–871. https://doi.org/10.1038/s41550-020-1095-2.

Borisov, G., 2019. MPEC, 2019-R106 (September 11).

Cheng, A.F., et al., 2008. Long-range reconnaissance imager on new Horizons. Space Sci. Rev. 140, 189–215. https://doi.org/10.1007/978-0-387-89518-5_9.

Cook, N.V., et al., 2016. Realistic detectability of close interstellar comets. Astrophys. J. 825, 51. https://doi.org/10.3847/0004-637X/825/1/51.

Cordiner, M.A., et al., 2020. Unusually high CO abundance of the first active interstellar comet. Nat. Astron. 4, 861–866. https://doi.org/10.1038/s41550-020-1087-2.

Davis, M.W., et al., 2021. The JUICE ultraviolet spectrograph: a next-generation compact UVS for ESA's JUICE mission. International Conference on Space Optics - ICSO 2020, 1185226. 11852.

Do, A., et al., 2018. Interstellar Interlopers: number density and origin of 'Oumuamualike objects. Astrophys. J. Lett. 855, L10. https://doi.org/10.3847/2041-8213/ aaae67.

El-Maarry, M.R., et al., 2019. Surface Morphology of comets and associated evolutionary processes: a review of Rosetta's observations of 67P/Churyumov-Gerasimenko. Space Sci. Rev. 215 https://doi.org/10.1007/s11214-019-0602-1.

- Engelhardt, T., et al., 2017. An observational upper limit on the interstellar number density of asteroids and comets. Astron. J. 153, 133. https://doi.org/10.3847/1538-3881/as588a
- Feldman, P.D., et al., 2007. Ultraviolet spectroscopy of comet 9P/Tempel 1 with Alice/ Rosetta during the Deep impact encounter. Icarus 187, 104. https://doi.org/ 10.1016/j.icarus.2006.08.016.
- Feldman, P.D., et al., 2015. Measurements of the near-nucleus coma of comet 67P/ Churyumov-Gerasimenko with the Alice far-ultraviolet spectrograph on Rosetta. Astron. Astrophys. 583, 8. https://doi.org/10.1051/0004-6361/201525925.
- Feldman, P.D., et al., 2016. The nature and frequency of the gas Outbursts in comet 67P/ Churyumov-Gerasimenko observed by the Alice far-ultraviolet spectrograph on Rosetta. Astrophys. J. Lett. 825, L8. https://doi.org/10.3847/2041-8205/825/1/L8.
- Fitzsimmons, A., et al., 2019. Detection of CN gas in interstellar object 2I/Borisov. Astrophys. J. Lett. 885, L9. https://doi.org/10.3847/2041-8213/ab49fc.
- Francis, P.J., 2005. The Demographics of long-period comets. Astrophys. J. 635, 1348. https://doi.org/10.1086/497684.
- Gladstone, G.R., et al., 2010. LAMP: the Lyman Alpha mapping project on NASA's lunar reconnaissance orbiter mission. Space Sci. Rev. 150, 161–181. https://doi.org/10.1007/s11214-009-9578-6
- Gladstone, G.R., et al., 2017. The ultraviolet spectrograph on NASA's Juno mission. Space Sci. Rev. 213, 447–473. https://doi.org/10.1007/s11214-014-0040-z.
- Grundy, W.M., et al., 2020. Color, composition, and thermal environment of Kuiper Belt object (486958) Arrokoth. Science 367, 6481. https://doi.org/10.1126/science. aav3705.
- Hoover, D.J., et al., 2022. The population of interstellar objects detectable with the LSST and Accessible for in situ rendezvous with various mission designs. The Planetary Science Journal 3, 71. https://doi.org/10.3847/PSJ/ac58fe.
- Ivezić, Z., et al., 2019. LSST: from science drivers to reference design and anticipated data Products. Astrophys. J. 873, 111. https://doi.org/10.3847/1538-4357/ab042c.
- Jewitt, D., 2015. Color Systematics of comets and related bodies. Astron. J. 150, 201. https://doi.org/10.1088/0004-6256/150/6/201.
- Jewitt, D., et al., 2017. Interstellar Interloper 11/2017 U1: observations from the NOT and WIYN telescopes. Astrophys. J. Lett. 850, L36. https://doi.org/10.3847/2041-8213/aa9b2f.
- Jewitt, D., Luu, J., 2019. Initial characterization of interstellar comet 2I/2019 Q4 (Borisov). Astrophys. J. Lett. 886, L29. https://doi.org/10.3847/2041-8213/
- Jewitt, D., et al., 2020. The nucleus of interstellar comet 2I/Borisov. Astrophys. J. Lett. 888, L23. https://doi.org/10.3847/2041-8213/ab621b.
- Knight, M.M., et al., 2017. On the rotation period and shape of the hyperbolic asteroid 11/'Oumuamua (2017 U1) from its Lightcurve. Astrophys. J. Lett. 851, L31. https://doi.org/10.3847/2041-8213/aa9d81.
- Marčeta, D., 2023. Synthetic population of interstellar objects in the Solar System. Astronomy and Computing 42, 100690, 2301.09375.
- Marčeta, D., Seligman, D.Z., 2023. Synthetic detections of interstellar objects with the Rubin observatory Legacy survey of space and time. Planet. Sci. J. 4, 230, 2310.17575.
- Marschall, R., et al., 2020. Cometary comae-surface Links. Space Sci. Rev. 216 https://doi.org/10.1007/s11214-020-00744-0.
- Mashchenko, S., 2019. Modelling the light curve of 'Oumuamua: evidence for torque and disc-like shape. Mon. Not. Roy. Astron. Soc. 489, 3003–3021. https://doi.org/10.1093/mnras/stz2380.
- McGlynn, T.A., Chapman, R.D., 1989. On the Nondetection of Extrasolar comets. Astrophys. J. Lett. 346, L105–L108. https://adsabs.harvard.edu/full/1989ApJ... 3461_105M
- McKinnon, W.B., et al., 2020. The solar nebula origin of (486958) Arrokoth, a primordial contact binary in the Kuiper Belt. Science 367, 6481. https://doi.org/10.1126/science.aay6620.

- Meech, K.J., et al., 2017. A brief visit from a red and extremely elongated interstellar asteroid. Nature 552, 378–381. https://doi.org/10.1038/nature25020.
- Meech, K.J., et al., 2023. Close up samples of exoplanetary systems: characterizing the next inter-stellar object. JWST Proposal. Cycle 2, 4116
- Moro-Martín, A., et al., 2009. Will the large Synoptic survey telescope detect Extra-solar planetesimals Entering the solar system? Astrophys. J. 704, 733–742. https://doi. org/10.1088/0004-637X/704/1/733.
- PrialniK, D., et al., 2004. Modeling the structure and activity of comet nuclei. In: Festou, M.C., Keller, H.U., Weaver, H.A. (Eds.), Comets II. University of Arizona Press, Tucson, pp. 359–387, 745. https://ui.adsabs.harvard.edu/abs/2004come. hook 350P
- Protopapa, S., et al., 2014. Water ice and dust in the innermost coma of comet 103P/ Hartley 2. Icarus 238, 191–204. https://doi.org/10.1016/j.icarus.2014.04.008.
- Protopapa, S., et al., 2018. Icy grains from the nucleus of comet C/2013 US10 (Catalina). Astrophys. J. 862 https://doi.org/10.3847/2041-8213/aad33b.
- Raponi, A., et al., 2020. Infrared detection of aliphatic organics on a cometary nucleus. Nat. Astron. 4, 500–505. https://doi.org/10.1038/s41550-019-0992-8.
- Reuter, D.C., et al., 2008. Ralph: a visible/infrared imager for the new Horizons Pluto/ Kuiper belt mission. Space Sci. Rev. 140, 129–154. https://doi.org/10.1007/s11214-008.9375.7
- Reuter, D.C., et al., 2023. L'Ralph: a visible/infrared spectral imager for the lucy mission to the Trojans. Space Sci. Rev. (in press).
- Sekanina, Z., 1976. A probability of encounter with interstellar comets and the likelihood of their existence. Icarus 27, 123–133. https://doi.org/10.1016/0019-1035(76)
- Seligman, D., Laughlin, G., 2018. The feasibility and Benefits of in situ exploration of 'Oumuamua-like objects. Astron. J. 155, 217. https://doi.org/10.3847/1538-3881/ aabd37.
- Snodgrass, C., Jones, G., 2019. The comet interceptor mission. Nat. Commun. 10, 5418.
- Stern, S.A., 1990. On the number of interstellar comets as a constraint on the formation rate of planetary systems. Proceedings of the Astronomical Society of the Pacific 102, 793. https://doi.org/10.1086/132704.
- Stern, S.A., et al., 2007. Alice: the Rosetta ultraviolet imaging spectrograph. Space Sci. Rev. 128, 507–527. https://doi.org/10.1007/s11214-006-9035-8.
- Stern, S.A., et al., 2008. Alice: the ultraviolet imaging spectrograph aboard the new Horizons Pluto-Kuiper belt mission. Space Sci. Rev. 140, 155–187. https://doi.org/ 10.1007/s11214-008-9407-3.
- Stern, S.A., et al., 2019. Initial results from the new Horizons exploration of 2014 MU69, a small Kuiper belt object. Science 364, 6441. https://doi.org/10.1126/science.aaw9771
- Stern, S.A., et al., 2023. The Properties and Origin of Kuiper Belt Object Arrokoth's Large Mounds. Planetary Sci. J. 4 https://doi.org/10.3847/PSJ/acf317.
- Vincent, J.-B., et al., 2019. Local Manifestations of cometary activity. Space Sci. Rev. 215 https://doi.org/10.1007/s11214-019-0596-8.
- Weaver, H.A., et al., 2008. Overview of the new Horizons science payload. Space Sci. Rev. 140, 75–91. https://doi.org/10.1007/s11214-008-9376-6.
- Weaver, H.A., et al., 2023. The lucy long range reconnaissance imager (L'LORRI). Space Sci. Rev. (in press).
- Williams, G., 2017. MPEC, 2017-U18.
- Williams, G.V., et al., 2017. Minor planets 2017 SN_33 and 2017 U1. Central Bureau Electronic Telegrams 4450, 1. https://ui.adsabs.harvard.edu/abs/2017CBET.4450....1W.
- Yang, B., et al., 2021. Compact pebbles and the evolution of volatiles in the interstellar comet 2I/Borisov. Nat. Astron. 5, 586–593. https://doi.org/10.1038/s41550-021-01336-w.